Available online at www.sciencedirect.com
SCIENCE DIRECT®
Journal of Sound and Vibration 284 (2005) 173–188
JOURNAL OF SOUND AND VIBRATION
www.elsevier.com/locate/jsvi

A method for the response of an elastic half-space to moving sub-Rayleigh point loads

Wen-I Liao[a,*], Tsung-Jen Teng[b], Chau-Shioung Yeh[c]

[a]*Department of Civil and Environmental Engineering, National University of Kaohsiung, No. 700, Kaohsiung University Road, Kaohsiung 811, Taiwan, ROC*
[b]*National Center for Research on Earthquake Engineering, Taipei, Taiwan, ROC*
[c]*Department of Civil Engineering, National Taiwan University, Taipei, Taiwan, ROC*

Received 15 May 2003; received in revised form 2 February 2004; accepted 11 June 2004
Available online 11 November 2004

Abstract

This paper presents the steady-state displacements and stresses in elastic half-space generated by a surface point load moving with constant speed parallel to the free surface of the half-space. The basic equations are solved by means of integral transforms, resulting in double fold integrals. A numerical technique is proposed to calculate the inner fold integral in wave number domain based on the method of steepest descent, and the time domain responses are obtained by Fourier synthesis over another wavenumber domain. Numerical results for displacement and stress components on the surface and within the half-space are presented for applied surface point loads with various subsonic speeds.

1. Introduction

The determination of vibratory motion on a free surface and the depth generated by moving vehicles has received considerable attention in the past. The fundamental problem of determining the response of a half-space subjected to a concentrated moving load with constant speed is also of interest because it can be applied to other important problems. For example, the study of the

*Corresponding author. Tel.: +886-75919-222; fax: +886-22732-2223.
E-mail address: wiliao@nuk.edu.tw (W.-I. Liao).

0022-460X/$ - see front matter © 2004 Elsevier Ltd. All rights reserved.
doi:10.1016/j.jsv.2004.06.005

surface vibration caused by moving vehicles, the seismic responses of a canyon subjected to obliquely incident waves, or the reduction of vibration induced by moving vehicles for an open trench can be accomplished by this fundamental solution.

The two-dimensional problem of a line force moving with constant subsonic velocity over the free surface of an elastic half-plane was first considered by Sneddon [1]. Cole and Huth [2] considered the same problem when the velocity of the applied force is in the subsonic, transonic and supersonic cases. An alternative approach to the high velocity was presented by Craggs [3]. Georgiadis and Barber [4] point out an error in the Cole/Huth solution, and rederive the correct Cole/Huth solution in the transonic range. The problem of a line force moving over the surface of a thick plate has been considered by Fulton and Sneddon [5] and Morley [6]. The transient problem for a load which is suddenly applied on the surface of an elastic half-space and then moves with constant velocity was considered by Payton [7,8].

The three-dimensional problem of the steady-state motion of a point load moving on the free surface has been considered by Papadopoulos [9] and Eason [10] with different approaches. Gakenheimer and Miklowitz [11] derived the transient responses in the interior of the elastic-space for a normal point load which is suddenly applied at a point and then moves with constant velocity along the free surface. Bakker et al. [12] revisited the same traveling point load problem, and used a more straightforward Cagniard technique than the work by Gakenheimer and Miklowitz [11] to obtain a solution, which allows greater insight into this important problem. Barber [13] used the Smirnov — Sobolev technique to obtain a closed form solution for normal displacements due to a normal point force moving at constant velocity over the surface of an elastic half-space. Georgiadis and Lykotrafitis [14] obtained fundamental elastodynamic three-dimensional solutions for loads moving steadily over the surface of a half-space based on the technique of the Radon (integral) transform and elements of distribution theory. de Barros and Luco [15] studied the steady-state responses within a multi-layered viscoelastic half-space generated by a buried or surface load moving parallel to the surface of the half-space. For some advanced applications, Georgiadis and Barber [16] examined the problem of the super-Rayleigh/subseismic elastodynamic indentation paradox, considering the asymptotic at the end of the contact region, and influence of contact inequalities. Brock and Georgiadis [17] proposed the asymptotic solution for the surface displacement and temperature due to a line mechanical/heat source that moves steadily over the surface of a half-space.

The present paper studies the steady-state response of elastic half-space subjected to a surface load moving with subsonic constant velocity in a fixed horizontal direction, and focuses on the study of the treatment for highly oscillating wave number integration. The approach proposed here is based on a two-fold integral representation of the complete response in terms of wavenumber. There are a variety of techniques for calculating the integral. Apsel and Luco [18] have proposed a technique for evaluation of the wavenumber integral by replacing the integral function with a quadratic polynomial, thus, resulting in a Filon-type quadrature. Kundu and Mal [19] have proposed an adaptive Gauss quadrature to accomplish the same task. Xu and Mal [20] have applied the Clenshaw–Curtis approach in which the integrand function is approximated with Chebyshev polynomials and then integrated to produce a Filon-type quadrature. In this paper, a numerical technique is proposed by using the modified steepest descent method to calculate the inner fold integral in wavenumber domain based on the modified method of steepest descent, which was proposed by Liao et al. [21,22] for the analysis of wave propagation in an elastic

half-space. In the present work, the numerical integration analysis looks like the previous work by Liao et al. [22], but for the moving load problem, the integrand in the integral differs from the previous work. Then the associated steepest descent path (SDP), location of the branch points and Rayleigh poles in the complex wavenumber domain appear in a different configuration compared to the previous work. It is also interesting to study the numerical integration analysis of the moving load problem in detail through the application of the modified steepest descent method. After replacing the original integral path by the SDP, the wavenumber integral results in a Gauss–Hermite-type quadrature, so that the oscillating character of the original integral can be removed and only the non-oscillating one needs to be evaluated. The final response in the time domain is obtained by Fourier synthesis over another wavenumber domain. Numerical results for stress and displacement components on the free surface and within the half-space with different moving load velocity are calculated and discussed.

2. Integral representation of the solution

Consider the half-space of a linear homogeneous isotropic elastic material with elastic constants λ, μ, and mass density ρ. The displacement field $\mathbf{u}$ is related to the displacement potential according to

$$\mathbf{u} = \nabla\phi + \nabla \times (0, \psi, 0) + \nabla \times \nabla \times (0, \chi, 0), \tag{1}$$

where ϕ is the longitudinal wave potential, and ψ and χ are the transverse wave potentials. The governing equations expressed by potentials are

$$\begin{aligned} c_p^2\nabla^2\phi - \ddot{\phi} &= 0, \\ c_s^2\nabla^2\psi - \ddot{\psi} &= 0, \\ c_s^2\nabla^2\chi - \ddot{\chi} &= 0, \end{aligned} \tag{2}$$

where $\nabla^2 = \partial^2/\partial x^2 + \partial^2/\partial y^2 + \partial^2/\partial z^2$ is the Laplacian operator, $c_p = \sqrt{(\lambda + 2\mu)/\rho}$ and $c_s = \sqrt{\mu/\rho}$ denote the longitudinal and transverse wave speeds, respectively. The surface of the half-space is free from tractions and radiation condition is imposed in the half-space. The point load with amplitude Q acts on the free surface and moves with velocity c along the y-axis passing through the origin point (0, 0, 0). The corresponding boundary conditions, e.g. a moving point load applied in the z-direction of the free surface, can be written as

$$\begin{aligned} \sigma_{zz}|_{z=0} &= -Q\delta(x)\delta(y - ct), \\ \sigma_{zx}|_{z=0} &= 0, \\ \sigma_{zy}\big|_{z=0} &= 0, \end{aligned} \tag{3}$$

where $\delta(x)$ represents Dirac's delta function. To solve the elastodynamic problem, Fourier transforms are applied to the governing equations with respect to time t, and with respect to horizontal coordinates x and y. Then Eq. (2) is transformed into

$$\frac{\mathrm{d}^2\bar{\varphi}}{\mathrm{d}z^2} + (k_p^2 - k_x^2 - k_y^2)\bar{\varphi} = 0, \tag{4a}$$

$$\frac{\mathrm{d}^2\bar{\psi}}{\mathrm{d}z^2} + (k_s^2 - k_x^2 - k_y^2)\bar{\psi} = 0, \tag{4b}$$

$$\frac{\mathrm{d}^2\bar{\chi}}{\mathrm{d}z^2} + (k_s^2 - k_x^2 - k_y^2)\bar{\chi} = 0, \tag{4c}$$

where k_p and k_s denote the longitudinal and transverse wavenumber, respectively. The resulting systems of ordinary differential equations with respect to the variable z are solved analytically with boundary conditions of Eq. (3), and the radiation condition. Then the resulting integral representations of displacement components are

$$u_x^\alpha = \frac{-Q}{8\pi^3\mu}\int_{-\infty}^{\infty}\int_{-\infty}^{\infty}\int_{-\infty}^{\infty}\delta(\omega - ck_y)[-\mathrm{i}k_x A^\alpha \mathrm{e}^{-\nu z} - \mathrm{i}k_y B^\alpha \mathrm{e}^{-\nu' z} + \mathrm{i}k_x \nu' C^\alpha \mathrm{e}^{-\nu' z}]\mathrm{e}^{-\mathrm{i}(k_x x + k_y y - \omega t)}\mathrm{d}k_x\,\mathrm{d}k_y\,\mathrm{d}\omega, \tag{5a}$$

$$u_y^\alpha = \frac{-Q}{8\pi^3\mu}\int_{-\infty}^{\infty}\int_{-\infty}^{\infty}\int_{-\infty}^{\infty}\delta(\omega - ck_y)[-\mathrm{i}k_y A^\alpha \mathrm{e}^{-\nu z} - \mathrm{i}k_x B^\alpha \mathrm{e}^{-\nu' z} + \mathrm{i}k_y \nu' C^\alpha \mathrm{e}^{-\nu' z}]\mathrm{e}^{-\mathrm{i}(k_x x + k_y y - \omega t)}\mathrm{d}k_x\,\mathrm{d}k_y\,\mathrm{d}\omega, \tag{5b}$$

$$u_z^\alpha = \frac{-Q}{8\pi^3\mu}\int_{-\infty}^{\infty}\int_{-\infty}^{\infty}\int_{-\infty}^{\infty}\delta(\omega - ck_y)[-\nu A^\alpha \mathrm{e}^{-\nu z} + k^2 C^\alpha \mathrm{e}^{-\nu' z}]\mathrm{e}^{-\mathrm{i}(k_x x + k_y y - \omega t)}\mathrm{d}k_x\,\mathrm{d}k_y\,\mathrm{d}\omega, \tag{5c}$$

where $k^2 = k_x^2 + k_y^2$, $\nu = \sqrt{k^2 - k_p^2}$, $\upsilon' = \sqrt{k^2 - k_s^2}$, In addition, the superscript $\alpha = x$, y or z denotes the direction of the applied moving load, for $\alpha = x$

$$A^x = \frac{2\mathrm{i}k_x\upsilon'}{F(k)}, \quad B^x = \frac{-\mathrm{i}k_y}{k^2\upsilon'}, \quad C^x = \frac{\mathrm{i}k_x(2k^2 - k_s^2)}{k^2F(k)}, \tag{6}$$

for $\alpha = y$

$$A^y = \frac{2\mathrm{i}k_y\upsilon'}{F(k)}, \quad B^y = \frac{\mathrm{i}k_x}{k^2\upsilon'}, \quad C^y = \frac{\mathrm{i}k_y(2k^2 - k_s^2)}{k^2F(k)}, \tag{7}$$

and for $\alpha = z$

$$A^z = \frac{2k^2 - k_s^2}{F(k)}, \quad B^z = 0, \quad C^z = \frac{2\upsilon}{F(k)}, \tag{8}$$

where

$$F(k) = (2k^2 - k_s^2)^2 - 4k^2\upsilon\upsilon'. \tag{9}$$

By inspection of Eqs. (5a)–(5c) the inversion of the Fourier transform with respect to ω can be done analytically leaving the response in the form of a double integral with respect to wavenumber in the x- and y-direction. Then Eqs. (5a)–(5c) yield

$$u_x^\alpha = \frac{-Q}{4\pi^2\mu}\int_{-\infty}^{\infty}\int_{-\infty}^{\infty}\left[-\mathrm{i}k_x A^\alpha \mathrm{e}^{-\upsilon z} - \mathrm{i}k_y B^\alpha \mathrm{e}^{-\upsilon' z} + \mathrm{i}k_x \upsilon' C^\alpha \mathrm{e}^{-\upsilon' z}\right]\mathrm{e}^{-\mathrm{i}(k_x x + k_y y')}\,\mathrm{d}k_x\mathrm{d}k_y, \tag{10a}$$

$$u_y^{\alpha} = \frac{-Q}{4\pi^2\mu}\int_{-\infty}^{\infty}\int_{-\infty}^{\infty}\left[-\mathrm{i}k_y A^{\alpha}\mathrm{e}^{-\upsilon z} - \mathrm{i}k_x B^{\alpha}\mathrm{e}^{-\upsilon' z} + \mathrm{i}k_y \upsilon' C^{\alpha}\mathrm{e}^{-\upsilon' z}\right]\mathrm{e}^{-\mathrm{i}(k_x x + k_y y')}\,\mathrm{d}k_x\,\mathrm{d}k_y, \tag{10b}$$

$$u_z^{\alpha} = \frac{-Q}{4\pi^2\mu}\int_{-\infty}^{\infty}\int_{-\infty}^{\infty}\left[-\upsilon A^{\alpha}\mathrm{e}^{-\upsilon z} + k^2 C^{\alpha}\mathrm{e}^{-\upsilon' z}\right]\mathrm{e}^{-\mathrm{i}(k_x x + k_y y')}\,\mathrm{d}k_x\,\mathrm{d}k_y, \tag{10c}$$

where $y' = y - ct$, and define parameters

$$M_p = c/c_p, \quad \beta_p = \sqrt{1 - M_p^2}, \tag{11a}$$

$$M_s = c/c_s, \quad \beta_s = \sqrt{1 - M_s^2}. \tag{11b}$$

Then the radical function υ and υ' can be rewritten as

$$\upsilon = \sqrt{k_x^2 + k_y^2\beta_p^2}, \tag{12a}$$

$$\upsilon' = \sqrt{k_x^2 + k_y^2\beta_s^2}. \tag{12b}$$

In this study, we restrict the moving load velocity, c, below the Rayleigh wave speed, c_R, of the elastic half-space. Then the parameters β_p and β_s are real numbers and the branch points of radical functions υ and υ' become pure imaginary numbers. Once the displacement functions have been determined, the corresponding Cartesian components of the stress fields are then calculated using the displacement–stress relationship. The wavenumber integrals over the k_x-domain are evaluated numerically through the application of the modified method of steepest descent. The application of this method to the moving load problem is presented in detail in the next section. Finally, the time domain response is obtained through the Fourier synthesis of the k_y-domain components by the Fourier transform algorithm.

3. Numerical integration

In view of the integral representations of displacements from Eqs. (10a)–(10c) and the associated stress fields, the integral for evaluation can be expressed as the general type:

$$I = \int_{-\infty}^{\infty} G_p(k_y)\,\mathrm{e}^{-\mathrm{i}k_y y'}\,\mathrm{d}k_y + \int_{-\infty}^{\infty} G_s(k_y)\,\mathrm{e}^{-\mathrm{i}k_y y'}\,\mathrm{d}k_y, \tag{13}$$

where

$$G_p(k_y) = \int_{-\infty}^{\infty} \frac{E_p(k_x, k_y, \upsilon, \upsilon')}{F(k_x, k_y, \upsilon, \upsilon')}\,\mathrm{e}^{-\upsilon z}\,\mathrm{e}^{-\mathrm{i}k_x x}\,\mathrm{d}k_x, \tag{14a}$$

$$G_s(k_y) = \int_{-\infty}^{\infty} \frac{E_s(k_x, k_y, \upsilon, \upsilon')}{F(k_x, k_y, \upsilon, \upsilon')}\,\mathrm{e}^{-\upsilon' z}\,\mathrm{e}^{-\mathrm{i}k_x x}\,\mathrm{d}k_x. \tag{14b}$$

To evaluate the inner fold integral over k_x-domain conventionally, the wavenumber k_x was firstly normalized by another wavenumber k_y, letting

$$\bar{k}_x = \frac{k_x}{k_y}. \tag{15}$$

Then the inner fold integral G_p and G_s becomes

$$G_p(k_y) = k_y \int_{-\infty}^{\infty} \frac{E_p(\bar{k}_x, k_y, \bar{\upsilon}, \bar{\upsilon}')}{F(\bar{k}_x, k_y, \bar{\upsilon}, \bar{\upsilon}')} \, \mathrm{e}^{-k_y(\bar{\upsilon}z + \mathrm{i}\bar{k}_x x)} \, \mathrm{d}k_x \tag{16a}$$

$$G_s(k_y) = k_y \int_{-\infty}^{\infty} \frac{E_s(\bar{k}_x, k_y, \bar{\upsilon}, \bar{\upsilon}')}{F(\bar{k}_x, k_y, \bar{\upsilon}, \bar{\upsilon}')} \, \mathrm{e}^{-k_y(\bar{\upsilon}'z + \mathrm{i}\bar{k}_x x)} \, \mathrm{d}k_x \tag{16b}$$

and the normalized radical functions $\bar{\upsilon}$ and $\bar{\upsilon}'$ are

$$\bar{\upsilon} = \sqrt{\bar{k}_x^2 + \beta_p^2}, \tag{17a}$$

$$\bar{\upsilon}' = \sqrt{\bar{k}_x^2 + \beta_s^2}. \tag{17b}$$

To illustrate the numerical procedure for calculating integral G_p and G_s in detail, let us consider the integral G_p first and adopt the cylindrical coordinate, which is shown in Fig. 1:

$$x = r \cos \theta, \tag{18a}$$

$$z = r \sin \theta. \tag{18b}$$

Defining the phase function $f_p(\bar{k}_x)$ associated with the integral G_p by

$$f_p(\bar{k}_x) = \mathrm{i}\bar{k}_x \cos \theta + \sqrt{\bar{k}_x^2 + \beta_p^2} \sin \theta \tag{19}$$

Eq. (16a) can be expressed as

$$G_p(k_y) = k_y \int_{-\infty}^{\infty} \frac{E_p(\bar{k}_x, k_y, \bar{\upsilon}, \bar{\upsilon}')}{F(\bar{k}_x, k_y, \bar{\upsilon}, \bar{\upsilon}')} \, \mathrm{e}^{-k_y f_p(\bar{k}_x) r} \, \mathrm{d}\bar{k}_x. \tag{20}$$

It can be observed that the integrand is highly oscillatory and the effort of integration depends on the location of the field point (r, θ) and the wavenumber, k_y. From the classical asymptotic analysis of the integral [23], the main contribution of the integral G_p comes from the saddle point

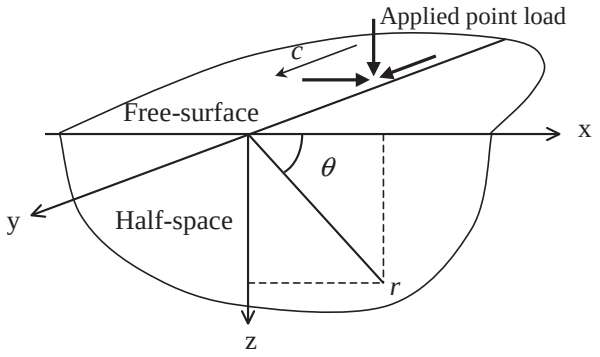

Fig. 1. Moving point load in an elastic half-space.

$\bar{k}_{op}$, which satisfies the condition

$$\left.\frac{\mathrm{d}f_p(\bar{k}_x)}{\mathrm{d}\bar{k}_x}\right|_{\bar{k}_x=\bar{k}_{op}} = 0. \tag{21}$$

Solving the above equation, we can find that the location of the saddle point depends on the location of the field point and is given by

$$\bar{k}_{op} = -\mathrm{i}\beta_p \cos\theta. \tag{22}$$

Based on the theory of complex variables, the original path of integration along the axis of real $\bar{k}_x$ can be deformed into a special equivalent path, namely, the SDP, which passes through the saddle point $\bar{k}_{op}$, and for all points in the SDP satisfies the following relation:

$$f_p(\bar{k}_x) - f_p(\bar{k}_{op}) = \tau^2, \tag{23}$$

where τ is a real variable. Then by solving Eq. (23) we can obtain the relationship between $\bar{k}_x$ and τ as

$$\bar{k}_x = -\mathrm{i}\cos\theta(\tau^2 + \beta_p) + \tau\sin\theta\sqrt{\tau^2 + 2\beta_p}. \tag{24}$$

The general form of the SDP is shown in Fig. 2. When the SDP does not encounter any branch cuts and no Rayleigh pole is enclosed within the contour, based on the Cauchy theorem and Jordan's lemma, the integral $G_p(k_y)$ shown in Eq. (20) will be equivalent to

$$G_p = k_y \mathrm{e}^{-rk_y\beta_p}\left[\int_{-\infty}^{\infty}\frac{E_p}{F}\,\mathrm{e}^{-rk_y\tau^2}\,\frac{\mathrm{d}\bar{k}_x}{\mathrm{d}\tau}\,\mathrm{d}\tau\right]. \tag{25}$$

Note that we have made use of the fact that

$$f_p(\bar{k}_{op}) = \beta_p \tag{26}$$

in the above derivation. It can be observed that along SDP the phase on each point remains stationary, and that the integral G_p behaves as a decaying wave. The merits of the above procedure are described as follows:

(a) The oscillating character that arises in the original integral has been removed from the integral. This results in an integral of the Hermite-type, which converges faster than the original one in view of the weighting factor $\mathrm{e}^{-rk_y\tau^2}$.
(b) The deformation of the original path into the steepest descent path is exact, and the only approximation comes from the truncation of the integral range, which depends on the values of k_y and r.
(c) The above procedure is valid uniformly either in the case of near to far field or in the case of low-to-high frequency.

Owing to the presence of the branch points $\pm\mathrm{i}\beta_p$, $\pm\mathrm{i}\beta_s$, and Rayleigh poles $\pm\mathrm{i}\beta_R$, where $\beta_R = \sqrt{1-(c/c_R)^2}$, and c_R is the Rayleigh wave speed, the SDP associated with integral G_p may encounter the branch cuts or enclose the Rayleigh pole. Taking this into consideration, the

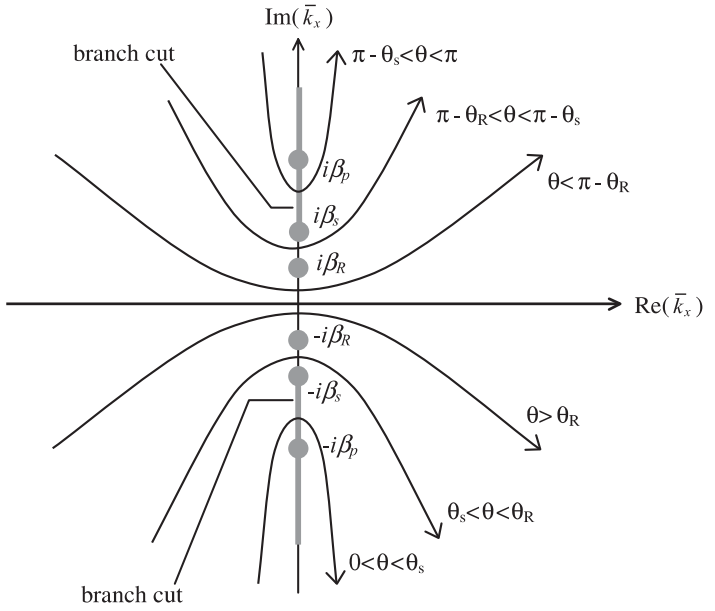

Fig. 2. The SDP for different angle θ in the complex $\bar{k}_x$-plane.

half-space is divided into the three regions as shown in Fig. 3, and denoted as region I–III. Their boundaries are specified by

(i) Region I: $\theta_R < \theta < \pi - \theta_R$, where $\theta_R = \cos^{-1}(\beta_R/\beta_p)$.
(ii) Region II: $\theta_s < \theta < \theta_R$ or $\pi - \theta_R < \theta < \pi - \theta_s$, where $\theta_s = \cos^{-1}(\beta_s/\beta_p)$.
(iii) Region III: $0 < \theta < \theta_s$ or $\pi - \theta_s < \theta < \pi$.

When a typical point is located in Region I, the associated SDP does not encounter any branch cuts and does not enclose the Rayleigh pole in the complex $\bar{k}_x$ – plane. The associated SDP is shown in Fig. 4(a). Therefore, the integral G_p can be evaluated by

$$G_p = k_y \mathrm{e}^{-rk_y\beta_p}\left[\int_{-\infty}^{\infty} \frac{E_p}{F}\,\mathrm{e}^{-rk_y\tau^2}\,\frac{\mathrm{d}\bar{k}_x}{\mathrm{d}\tau}\,\mathrm{d}\tau\right]. \tag{27}$$

For a typical point located in Region II, the associated SDP shown in Fig. 4(b) will enclose the Rayleigh pole will not encounter any branch cuts. Then the integral G_p is equivalent to

$$\begin{aligned} G_p = {} & k_y \mathrm{e}^{-rk_y\beta_p}\left[\int_{-\infty}^{\infty} \frac{E_p}{F}\,\mathrm{e}^{-rk_y\tau^2}\,\frac{\mathrm{d}\bar{k}_x}{\mathrm{d}\tau}\,\mathrm{d}\tau\right] \\ & - \mathrm{sgn}(\cos\,\theta)2\pi\mathrm{i}\left.\frac{E_p}{F'}\right|_{\bar{k}_x=-\mathrm{sgn}(\cos\,\theta)\,\mathrm{i}\beta_R} \mathrm{e}^{-k_y(\bar{v}_R z+\beta_R x\,\mathrm{sgn}(\cos\,\theta))}, \end{aligned} \tag{28}$$

where

$$F' = \frac{\mathrm{d}F(\bar{k}_x)}{\mathrm{d}\bar{k}_x} = k_y^2\left[8\bar{k}_x(2k^2 - k_y^2(M_s^2 + \bar{v}\bar{v}') - 4\bar{k}_x k^2\left(\frac{\bar{v}}{\bar{v}'} + \frac{\bar{v}'}{\bar{v}}\right)\right] \tag{29}$$

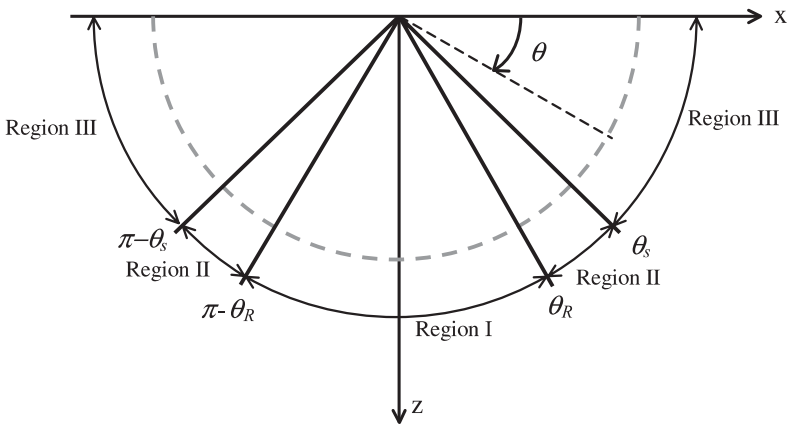

Fig. 3. The regions where the contribution of branch cut or pole should be taken into account or not taken into account for the integral G_p.

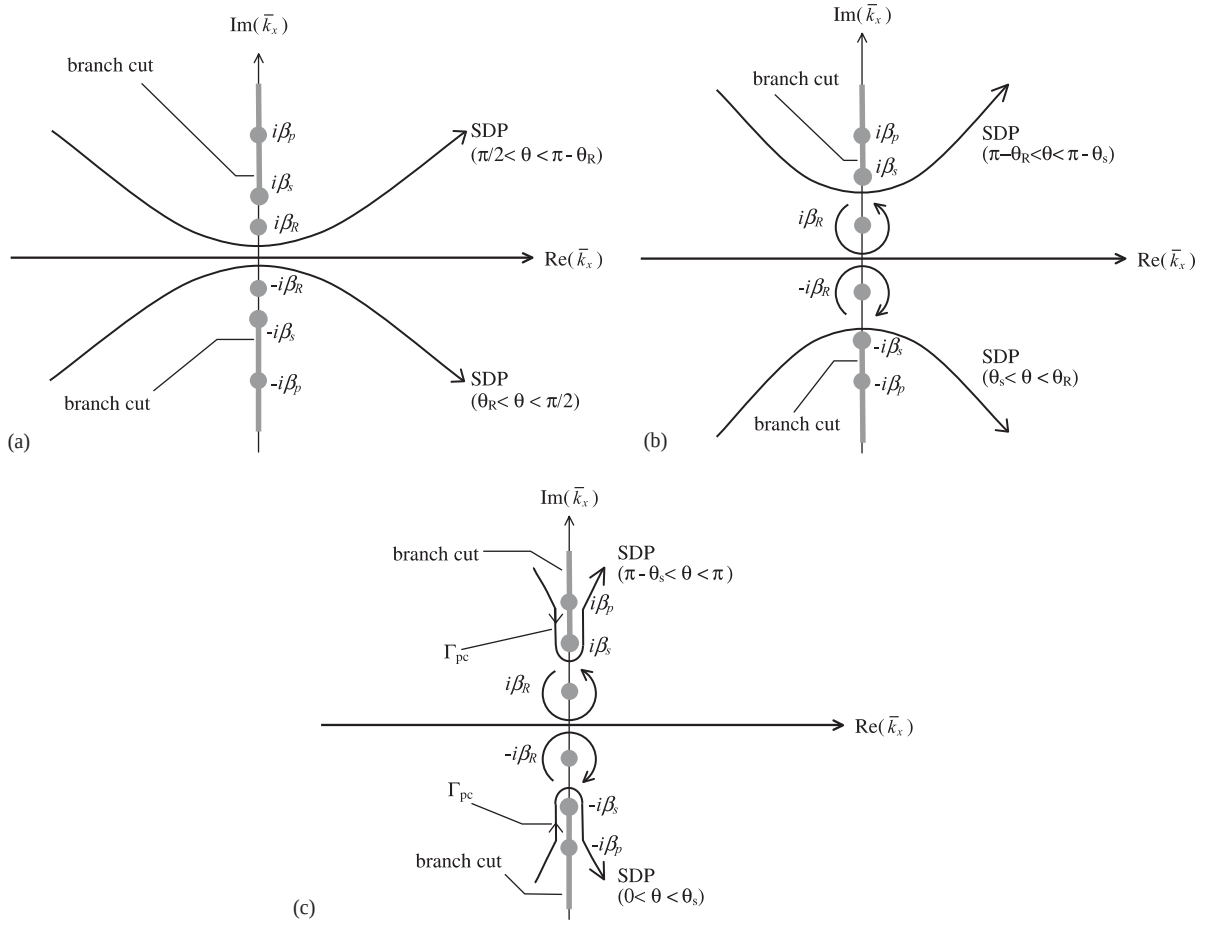

Fig. 4. The SDP associated with integral G_p for the field point located in (a) region I; (b) region II; (c) region III.

and

$$\bar{v}_R = \sqrt{\beta_p^2 - \beta_R^2} \tag{30}$$

The same should be considered for a typical field point located in Region III. The SDP encloses the Rayleigh pole and intersects the branch cut of radical function $\bar{v}'$ (branch points $\pm i\beta_s$). Therefore, a return loop must be added to account for the contribution from the branch cut. The return loop shown in Fig. 4(c) comes from the saddle point $\bar{k}_{op}$, passes around the branch point $\pm i\beta_s$ in the proper manner, and returns to the saddle point. Then the integral G_p is equivalent to

$$\begin{aligned} G_p = {} & k_y e^{-rk_y\beta_p}\left[\int_{-\infty}^{\infty} \frac{E_p}{F} e^{-rk_y\tau^2} \frac{d\bar{k}_x}{d\tau} d\tau\right] \\ & - \operatorname{sgn}(\cos\theta) 2\pi i \left.\frac{E_p}{F'}\right|_{\bar{k}_x=-\operatorname{sgn}(\cos\theta)i\beta_R} e^{-k_y(\bar{v}_R z+\beta_R x \operatorname{sgn}(\cos\theta))} \\ & + k_y \int_{\Gamma_{pc}} \frac{E_p}{F} e^{-k_y(\bar{v}z+i\bar{k}_x x)} d\bar{k}_x, \end{aligned} \tag{31}$$

where Γ_{pc} denotes the return loop along the branch cut of the radical function $\bar{v}'$.

For the integral G_s, the same consideration as for the integral G_p should be made. The phase function $f_s(\bar{k}_x)$ associated with the integral G_s is

$$f_s(\bar{k}_x) = i\bar{k}_x \cos\theta + \sqrt{\bar{k}_x^2 + \beta_s^2}\sin\theta. \tag{32}$$

The original path is also deformed into a SDP with respect to the integral G_s, so all points in the steepest descent path (SDP) satisfy the relationship

$$f_s(\bar{k}_x) - f_s(\bar{k}_{os}) = \tau^2 \tag{33}$$

where $\bar{k}_{os} = -i\beta_s \cos\theta$ is the saddle point with respect to the phase function $f_s(\bar{k}_x)$. From Eq. (33), the relationship between $\bar{k}_x$ and the real variable τ can be written as

$$\bar{k}_x = -i\cos\theta(\tau^2 + \beta_s) + \tau\sin\theta\sqrt{\tau^2 + 2\beta_s}. \tag{34}$$

In view of the location of the saddle point $\bar{k}_{os} = -i\beta_s\cos\theta\,(0 \leqslant \theta \leqslant \pi)$, it is very straightforward to know that the SDP may enclose the Rayleigh pole but will absolutely not encounter any branch cuts. Thus, the half-space is divided into two regions as shown in Fig. 5, and denoted as Regions I and II. The associated SDP with respect to Regions I and II are shown in Fig. 6(a) and (b), respectively. Their boundaries and equivalent integrals G_s are expressed as follows:

(a) Region I, $\theta_R^* < \theta < \pi - \theta_R^*$

$$G_s = k_y e^{-rk_y\beta_s}\left[\int_{-\infty}^{\infty} \frac{E_s}{F} e^{-rk_y\tau^2} \frac{d\bar{k}_x}{d\tau} d\tau\right], \tag{35}$$

where $\theta_R^* = \cos^{-1}(\beta_R/\beta_s)$.

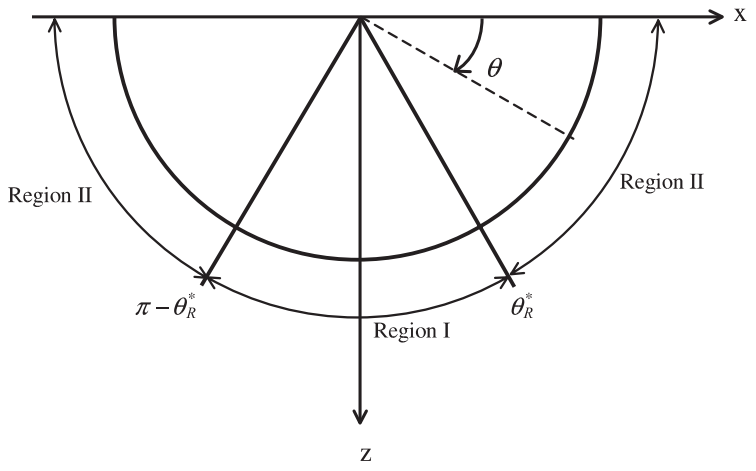

Fig. 5. The regions where the contribution of the pole should be taken into account or not taken into account for the integral G_s.

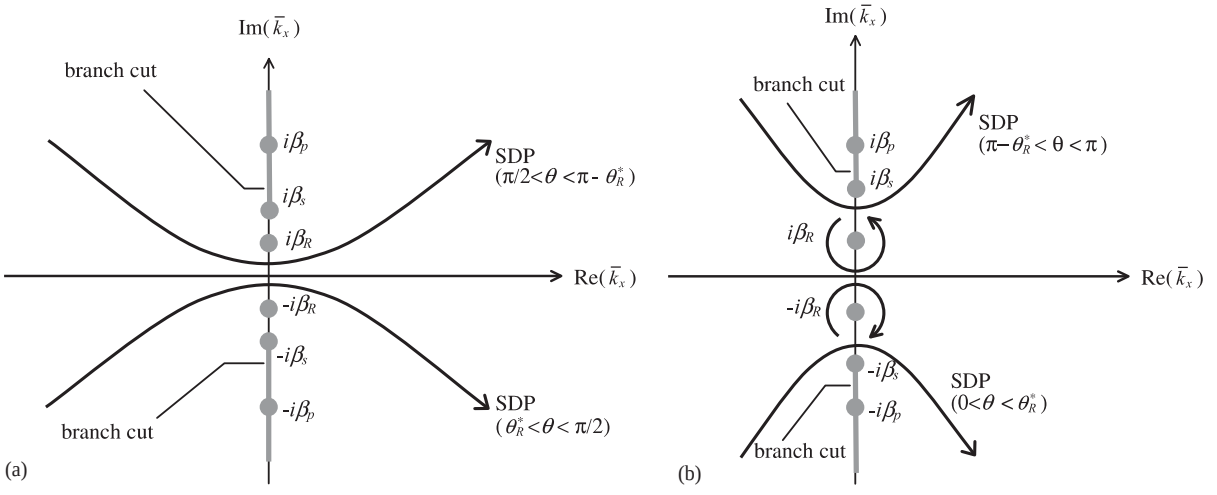

Fig. 6. The SDP associated with integral G_s for the field point located in (a) region I; (b) region II.

(b) Region II, $\theta<\theta_R^*$ or $\theta>\pi-\theta_R^*$

$$G_s = k_y e^{-rk_y\beta_s}\left[\int_{-\infty}^{\infty}\frac{E_s}{F}e^{-rk_y\tau^2}\frac{d\bar{k}_x}{d\tau}\,d\tau\right] - \operatorname{sgn}(\cos\theta)2\pi i\frac{E_s}{F'}\bigg|_{\bar{k}_x=-\operatorname{sgn}(\cos\theta)i\beta_R} e^{-k_y(\bar{v}_R'z+\beta_R x\,\operatorname{sgn}(\cos\theta))} \tag{36}$$

where $\bar{v}_R' = \sqrt{\beta_s^2-\beta_R^2}$.

After obtaining the integral value G_p and G_s in the k_x wavenumber domain by the modified steepest descent method, the final response in the time domain can be obtained by Fourier synthesis over the k_y wavenumber domain.

4. Numerical Results

The shape of displacement and stress pulses at a station of an elastic half-space subjected to a surface point load moving along the positive y-axis are shown in Figs. 7(a)–(c). The numerical results were calculated for an elastic half-space characterized by $c_p = 1732$ and $c_s = 1000$ m/s. For all figures, the Gaussian integral points aligned on the SDP are 128 points if the field point of integral G_p is located in Region I, and 256 points if the field point is located in Region II or III. For the integral G_s, the Gaussian integral points aligned on the SDP are 128 points for Region I, and 256 points for Region II. In these figures, the dimensionless displacement $U=(\mu r/Q)u$ and the stress $S=(r^2/Q)\sigma$ components are plotted against the dimensionless time $t^* = c_s t/r$, where Q is the amplitude of the applied moving load, r is the radial distance from the observation point to the origin of the half-space, u is the displacement component, and σ is the stress component. The instant $t=0$ corresponds to the time at which the point load passes through the coordinate $y=0$. In Figs. 7(a)–(c), the superscript of displacement and stress components denotes the direction in which the point load is applied. Displacement and stress components shown in Figs. 7(a)–(c) correspond to a subsonic load velocity 700 m/s ($M_s = 0.7$) in the observation point located at (x, y, z) = (0,0,10 m). The comparison of displacement components by the present method with those obtained by de Barros and Luco [15] is shown in Fig. 7(a), and it can be seen that the comparison is excellent.

Fig. 8 shows the attenuation curve for maximum displacement amplitude in the three direction of the free surface along the x-axis generated by a vertical load with moving velocity $c = 100$ m/s ($M_s = 0.1$), 400 m/s ($M_s = 0.4$) and 700 m/s ($M_s = 0.7$), respectively. From those figures, the attenuated properties of maximum displacement along x-axis are observed and show that the larger M_s causes a larger maximum displacement at all points along the x-axis.

5. Concluding Remarks

This paper presents a procedure for the analysis of steady-state response in elastic half-space generated by a surface sub-Rayleigh point load moving with constant speed. Results are presented

Fig. 7. (a) Normalized displacement components at an observation point (x,y,z) = (0,0,10 m) for a point load moving with velocity ($M_s = 0.7$) along the positive y-axis over the surface of an elastic half-space, while displacements obtained by de Barros and Luco [15] are shown with circles. The superscript denotes the direction of the point load. (b,c) Normalized stress components at an observation point (x,y,z) = (0,0,10 m) for a point load moving with velocity ($M_s = 0.7$) along the positive y-axis over the surface of an elastic half-space. The superscript denotes the direction of the point load.

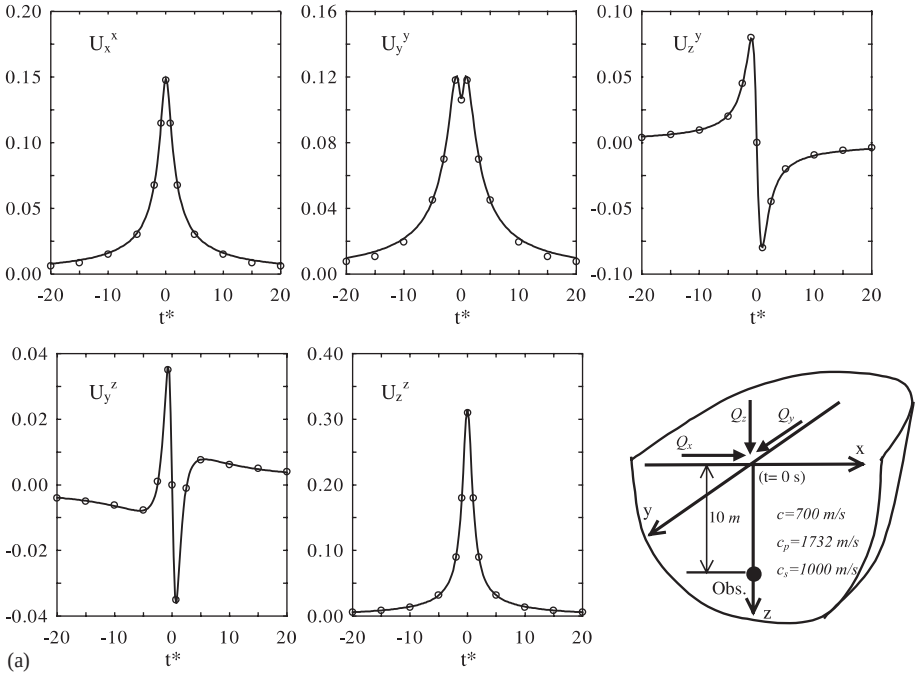
U_x^x
U_y^y
U_z^y
U_y^z
U_z^z
t*
Q_z
Q_y
Q_x
x
y
z
(t= 0 s)
10 m
c=700 m/s
c_p=1732 m/s
c_s=1000 m/s
Obs.
(a)

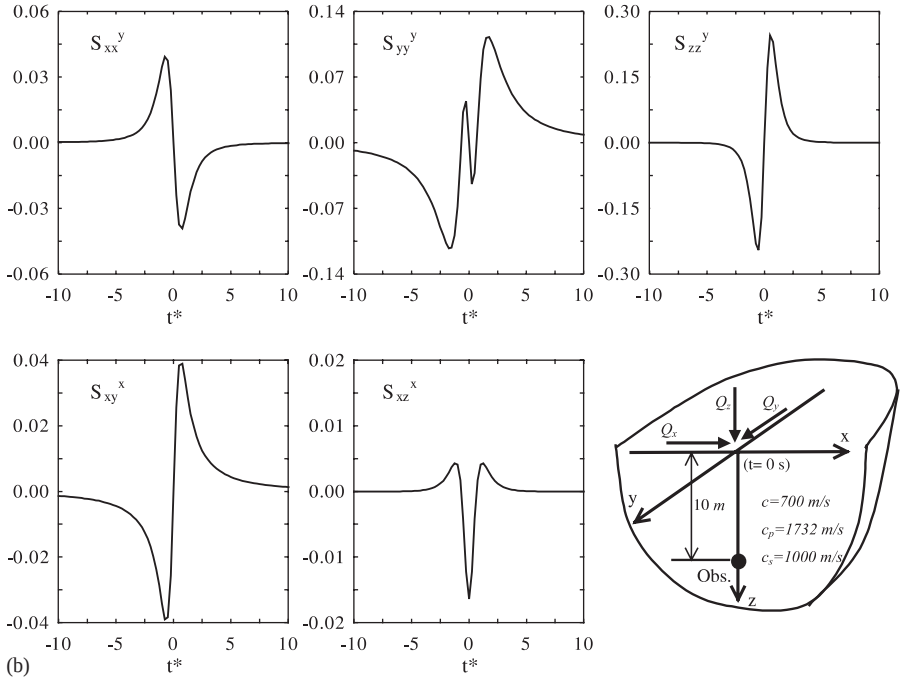
S_{xx}^y
S_{yy}^y
S_{zz}^y
S_{xy}^x
S_{xz}^x
t*
Q_z
Q_y
Q_x
x
y
z
(t= 0 s)
10 m
c=700 m/s
c_p=1732 m/s
c_s=1000 m/s
Obs.
(b)

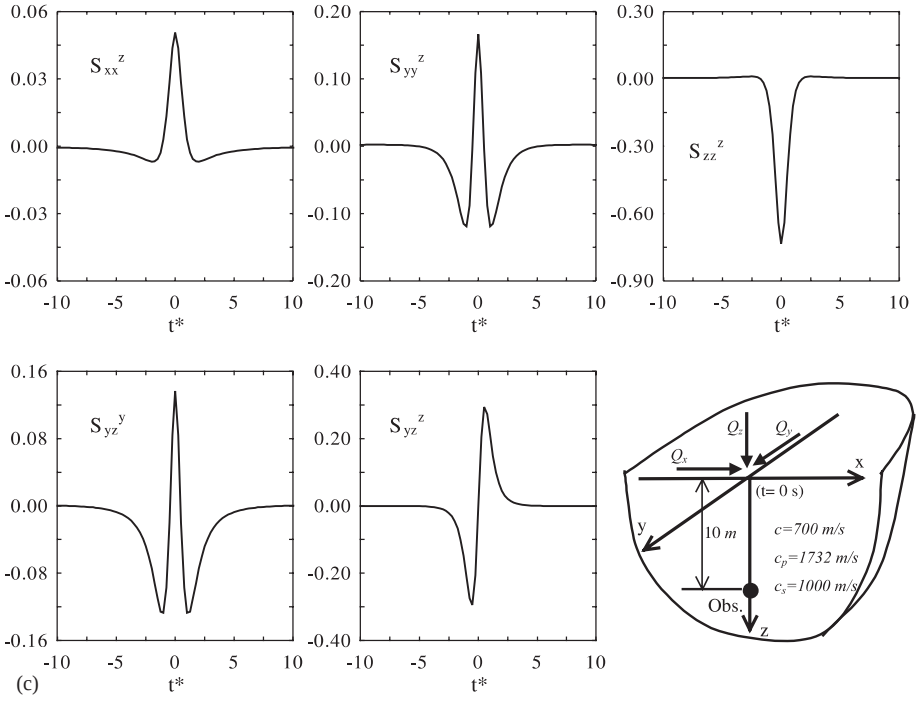

Fig. 7. (*Continued*)

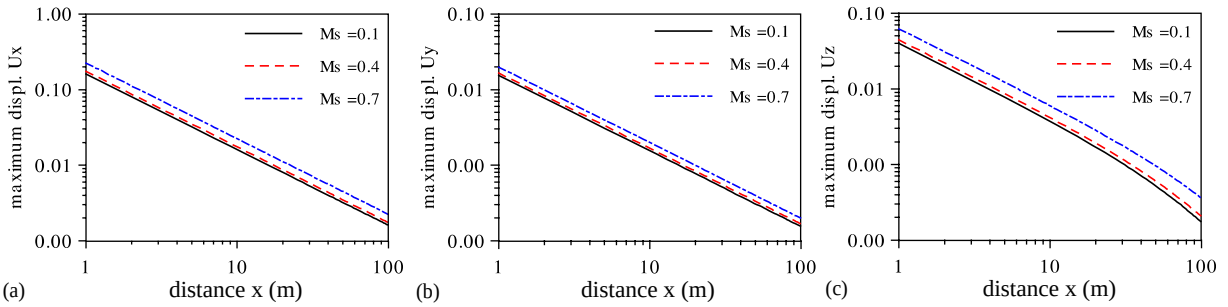

Fig. 8. Attenuation curves for maximum amplitudes of: (a) x-direction; (b) y-direction; and (c) z-direction displacements on the free surface along the x-axis by a vertical point load moving with velocity 100, 400 and 700 m/s, respectively.

for displacement and stress components on the surface and within the elastic half-space with different observation points and load velocities. A technique is proposed to calculate the integral in wavenumber domain based on the method of steepest descent. After replacing the original integration path by the steepest descent path, the wavenumber integral results in a Gauss–Hermite-type quadrature, and with non-oscillating integrand, it is very helpful in computing efficiency. It is expected that the fundamental solution of the moving load problem

presented here can be applied to certain applications in radiation, scattering and interaction problems associated with moving disturbances.

Acknowledgements

The authors gratefully acknowledge the financial support granted by the National Science Council, ROC. The facility of calculation provided by the National Center for Research on Earthquake Engineering, ROC, is also highly appreciated.

References

[1] I.N. Sneddon, *Fourier Transforms*, McGraw-Hill, New York, 1951.
[2] J. Cole, J. Huth, Stress produced in a half-space by moving loads, *Journal of Applied Mechanics* 25 (1958) 433–436.
[3] J.W. Craggs, Two dimensional waves in an elastic half-space, *Proceedings of the Cambridge Philosophical Society* 56 (1960) 269–275.
[4] H.G. Georgiadis, J.R. Barber, Steady-state transonic motion of a line load over an elastic half-space: The corrected Cole–Huth solution, *Journal of Applied Mechanics* 60 (1993) 772–774.
[5] J. Fulton, I.N. Sneddon, The dynamic stresses produced in a thick plate by the action of surface forces, *Proceedings of the Glasgow Mathematical Association* 3 (1958) 153–168.
[6] L.S.D. Morley, Elastic plate with loads travelling at uniform velocity along the bounding surface, *Quarterly Journal of Applied Mathematics* 15 (1962) 193–213.
[7] R.G. Payton, An application of the dynamic Betti–Rayleigh reciprocal theorem to moving-point loads in elastic media, *Quarterly Journal of Applied Mathematics* 21 (1964) 299–313.
[8] R.G. Payton, Transient motion of an elastic half-space due to a moving line load, *International Journal of Engineering Science* 5 (1967) 49–79.
[9] M. Papadopoulos, The elastodynamics of moving loads, *Journal of the Australian Mathematical Society* 3 (1963) 79–92.
[10] G. Eason, The stress produced in a semi-infinite solid by moving surface force, *International Journal of Engineering Science* 2 (1965) 581–609.
[11] D.C. Gakenheimer, J. Miklowitz, Transient excitation of an elastic half-space by a point load travelling on the surface, *Journal of Applied Mechanics* 36 (1969) 505–515.
[12] M.C.M. Bakker, M.D. Verweij, B.J. Kooij, H.A. Dieterman, The traveling point load revisited, *Wave Motion* 29 (1999) 119–135.
[13] J.R. Barber, Surface displacements due to a steadily moving point force, *Journal of Applied Mechanics* 63 (1996) 245–251.
[14] H.G. Georgiadis, G. Lykotrafitis, A method based on the Radon transform for three-dimensional elastodynamic problems of moving loads, *Journal of Elasticity* 65 (2001) 87–129.
[15] F.C.P. de Barros, J.E. Luco, Response of a layered viscoelastic half-space to a moving point load, *Wave Motion* 19 (1994) 189–210.
[16] H.G. Georgiadis, J.R. Barber, On the super-Rayleigh/subseismic elastodynamic indentation problem, *Journal of Elasticity* 31 (1993) 141–161.
[17] L.M. Brock, H.G. Georgiadis, Steady-state motion of a line mechanical/heat source over a half-space: a thermoelastodynamic solution, *Journal of Applied Mechanics* 64 (1997) 562–567.
[18] R.J. Apsel, J.E. Luco, On the Green's function for a layered half-space: Part II, *Bulletin of the Seismological Society of America* 73 (1983) 931–951.
[19] T. Kundu, A.K. Mal, Elastic waves in multilayered solids due to a dislocation source, *Wave Motion* 7 (1985) 459–471.

[20] P.C. Xu, A.K. Mal, An adaptive scheme for irregularly oscillatory functions, *Wave Motion* 7 (1985) 235–243.
[21] W.I. Liao, Dynamic Responses of an Elastic-Half Space with Defect Subjected to Elastic Waves, PhD Thesis, National Taiwan University, 1997.
[22] W.I. Liao, T.J. Teng, C.S. Yeh, A series solution and numerical technique for wave diffraction by a three-dimensional canyon, *Wave Motion* 39 (2004) 129–142.
[23] J.D. Achenbach, *Wave Propagation in Elastic Solids*, North-Holland, Amsterdam, 1973.